Supplementary information

Carbonation Induced Structural Changes in Soil-Based Alkali-Activated Binders

Nikita Rao,[1,†] Pitabash Sahoo,[2,†] P.S.V.R.A Kishor,[3] Adarsh Pathiyath,[3] Aslam Kunhi Mohamed,[3] Souradeep Gupta,[2] Amrit Venkatesh,[4] Sheetal K. Jain[1,*]

[1]Solid State and Structural Chemistry Unit, Indian Institute of Science, Bengaluru, India

[2]Centre for Sustainable Technology, Indian Institute of Science, Bengaluru, India

[3]Department of Civil Engineering, Indian Institute of Technology Madras, Chennai, India

[4]National High Magnetic Field Laboratory, Florida State University, Tallahassee, Florida 32310, United States

†N. Rao and P. Sahoo contributed equally to this work

*E-mail: skj@iisc.ac.in

This file includes:

Supplementary Figures S1-S13

Supplementary Tables S1-S7

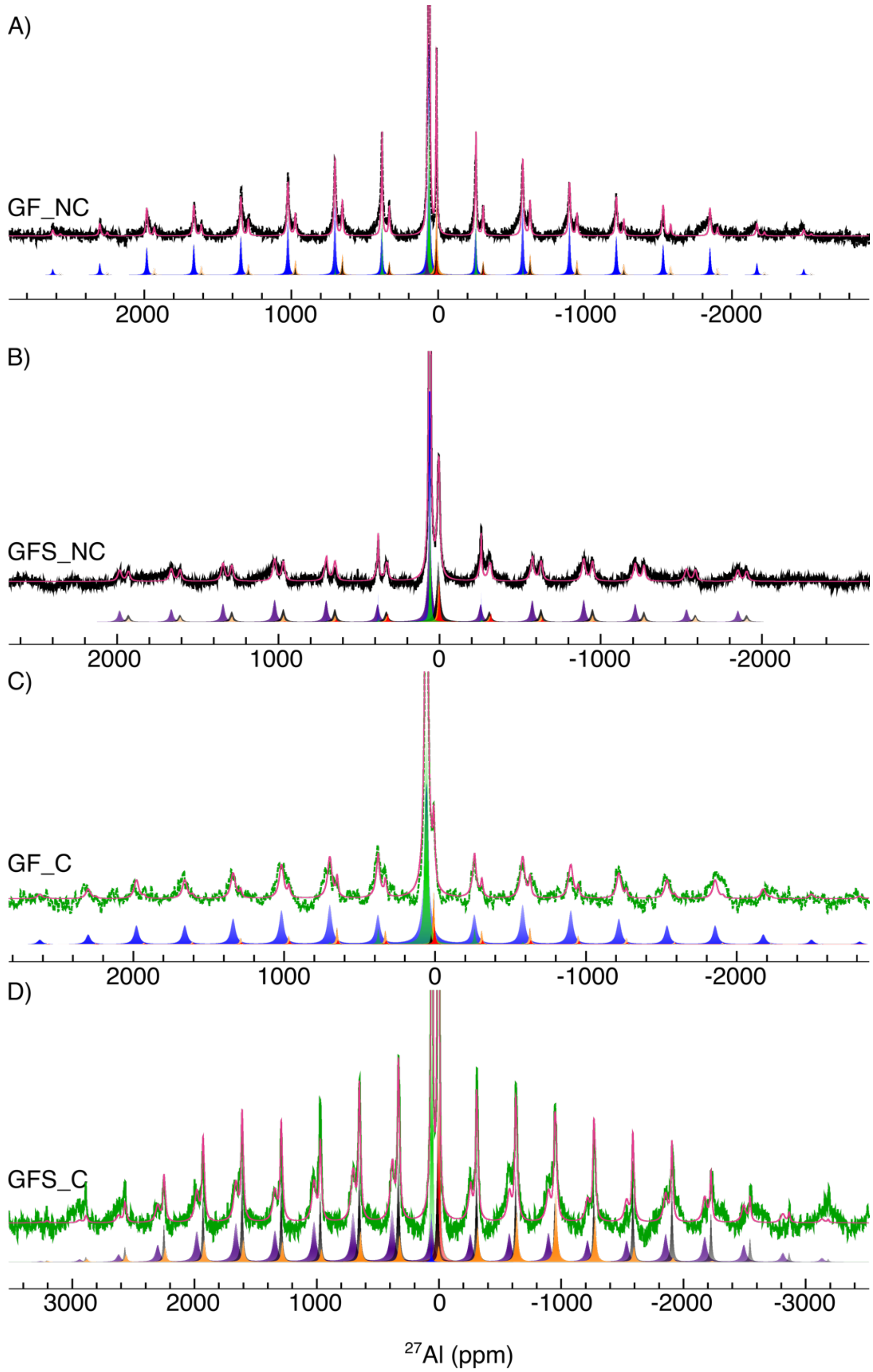

Fig. S1. Fitted ^{27}Al MAS NMR spectrum of the GF_NC sample.

^{27}Al MAS NMR spectra (blue line) of the GF_NC sample, with the fitted spectrum shown in red. The inset highlights the isotropic region, where six components were used for deconvolution: three peaks corresponding to Al(IV) and three to Al(VI) sites. Fit parameters are detailed in Table S1. The full spectrum illustrates the spinning sideband pattern fitted using the quadrupolar (quad) and chemical shift anisotropy (CSA) models. The spectra were acquired at 9.4 T and 33.33 kHz MAS

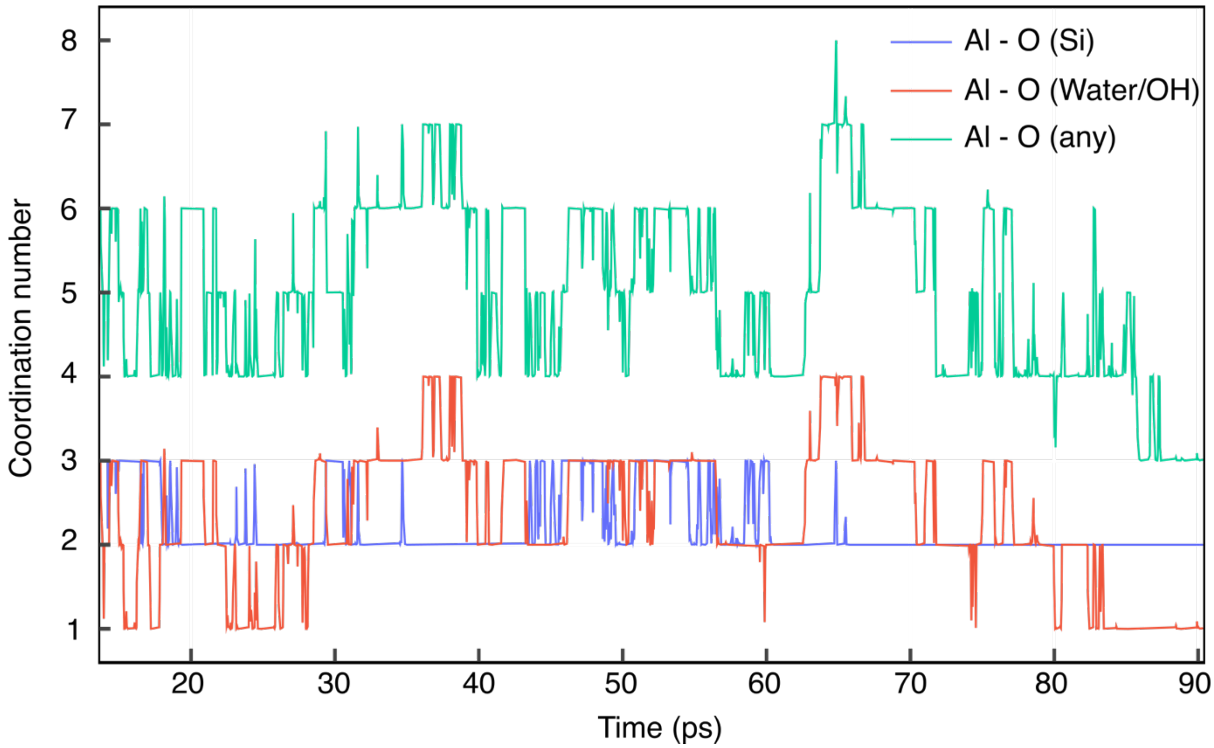

Fig. S2. Coordination numbers (CN) of aluminum with different species as a function of time. Here, we can observe that the chosen bias factor is probably too high to explore the different CN for aluminum and this could be optimized (for efficient computing) for a larger set of structures to avoid CN<4 or >6. This is beyond the scope of this work.

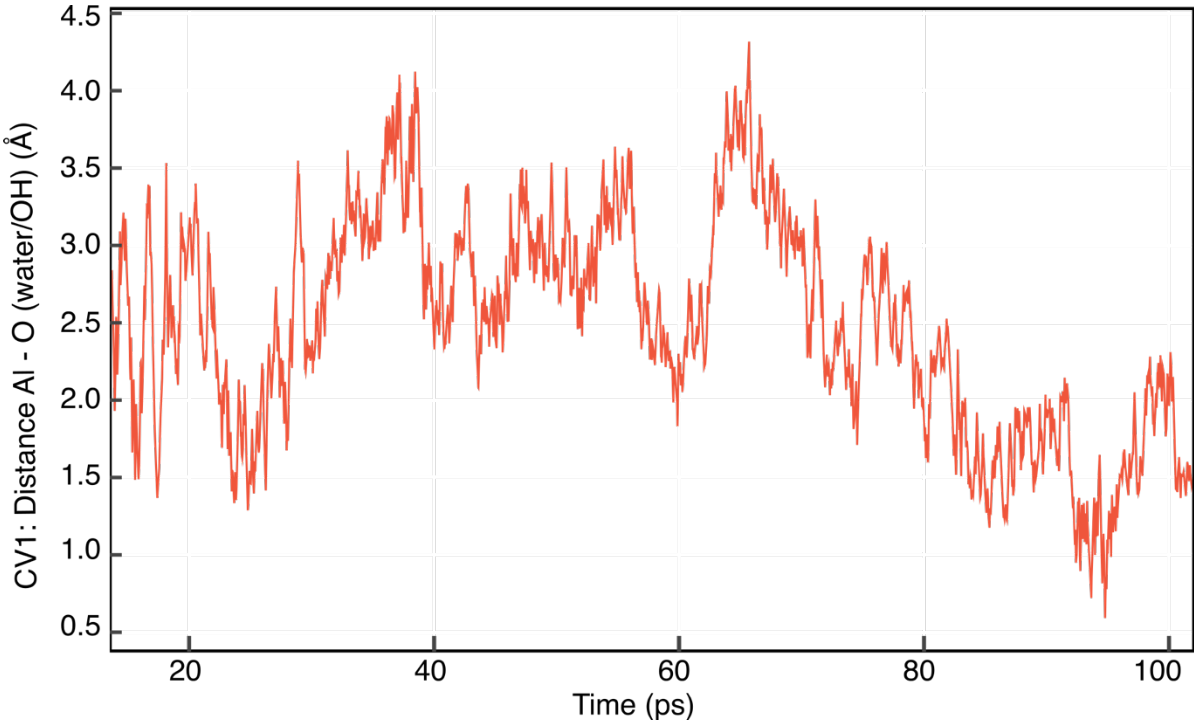

Fig. S3. Collective variable 1 as a function of time.
CV1 is the number of oxygen atoms belonging to a water molecule or hydroxyl which are less than 0.23 nm away from the aluminum atom in the C-A-S-H structure considered.

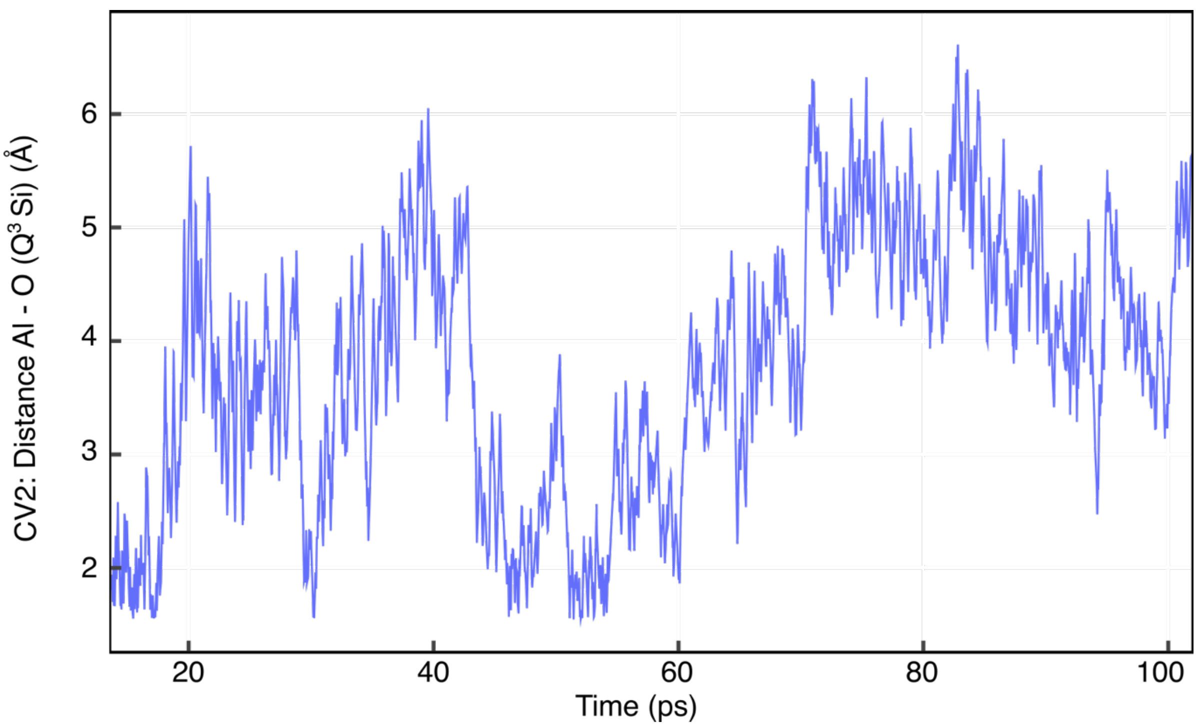

Fig. S4. Collective variable 2 as a function of time.
CV2 is the distance between the aluminum atom and the oxygen of the bridging silicon in the other chain, making a cross-linking if it is bonded to the aluminum.

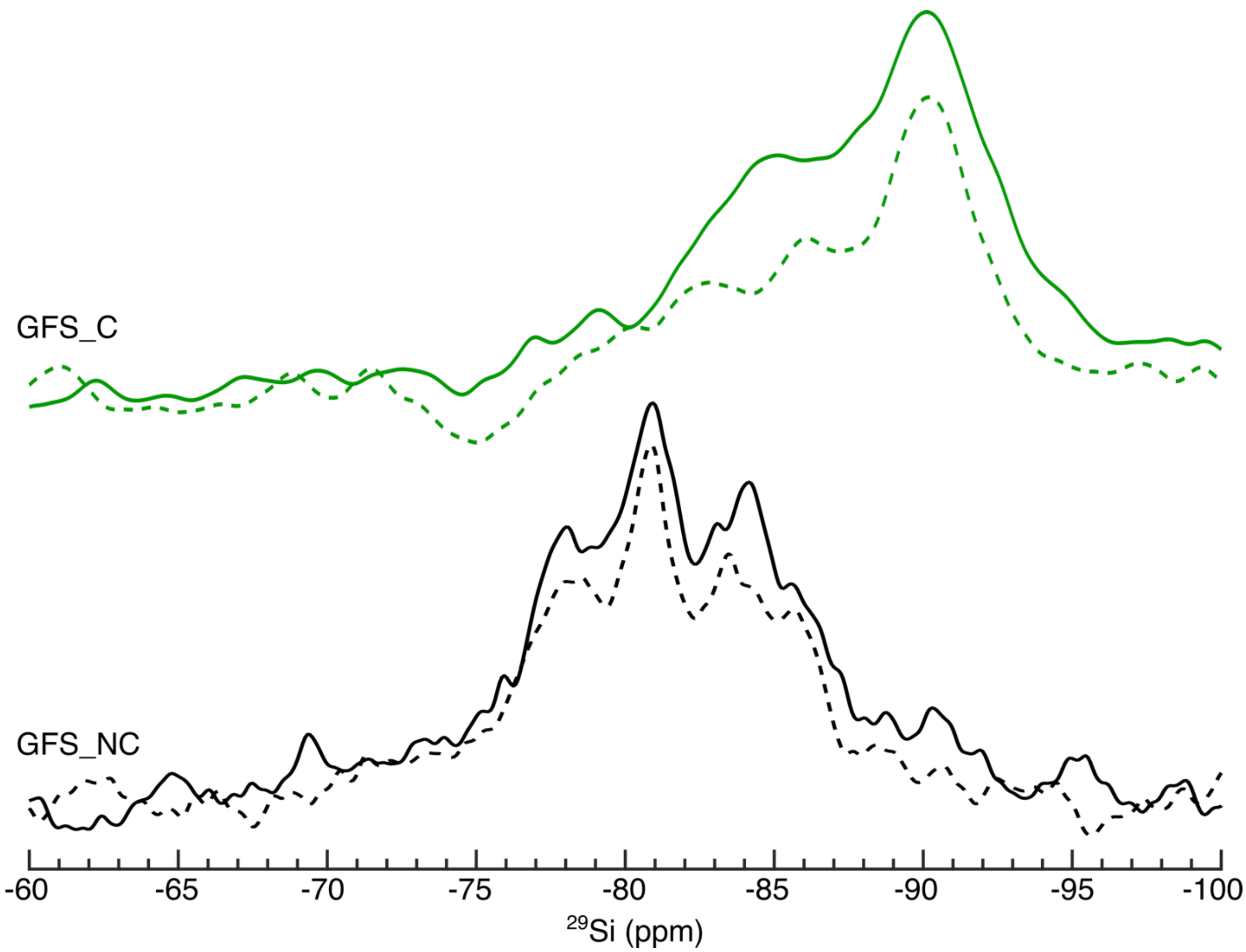

Fig. S5. $^{29}Si\{^{27}Al\}$ RESPDOR spectra for GFS samples.
R-RESPDOR (rotation echo saturation pulse double resonance)[1] reference spectrum (S_0) are shown using solid lines while the dashed lines represent the dephased spectrum (S) are shown in dashed lines and the GFS in solid lines. The spectra were acquired at 18.8 T magnetic field and 16 kHz MAS at the National High Magnetic Field Laboratory (NHMFL). RESPDOR spectra were acquired by direct excitation of ^{29}Si signals followed by rotary resonance recoupling (R^3) at 16 kHz rf power. ^{29}Si $\pi/2$ and π pulse lengths of 6 and 12 μs, respectively, were used. A 1.5× rotor period saturation pulse was applied on the ^{27}Al channel at ca. 40 kHz rf power. The total dipolar recoupling duration was set to 64 rotor cycles. 32,768 scans and a 1 s recycle delay was used.

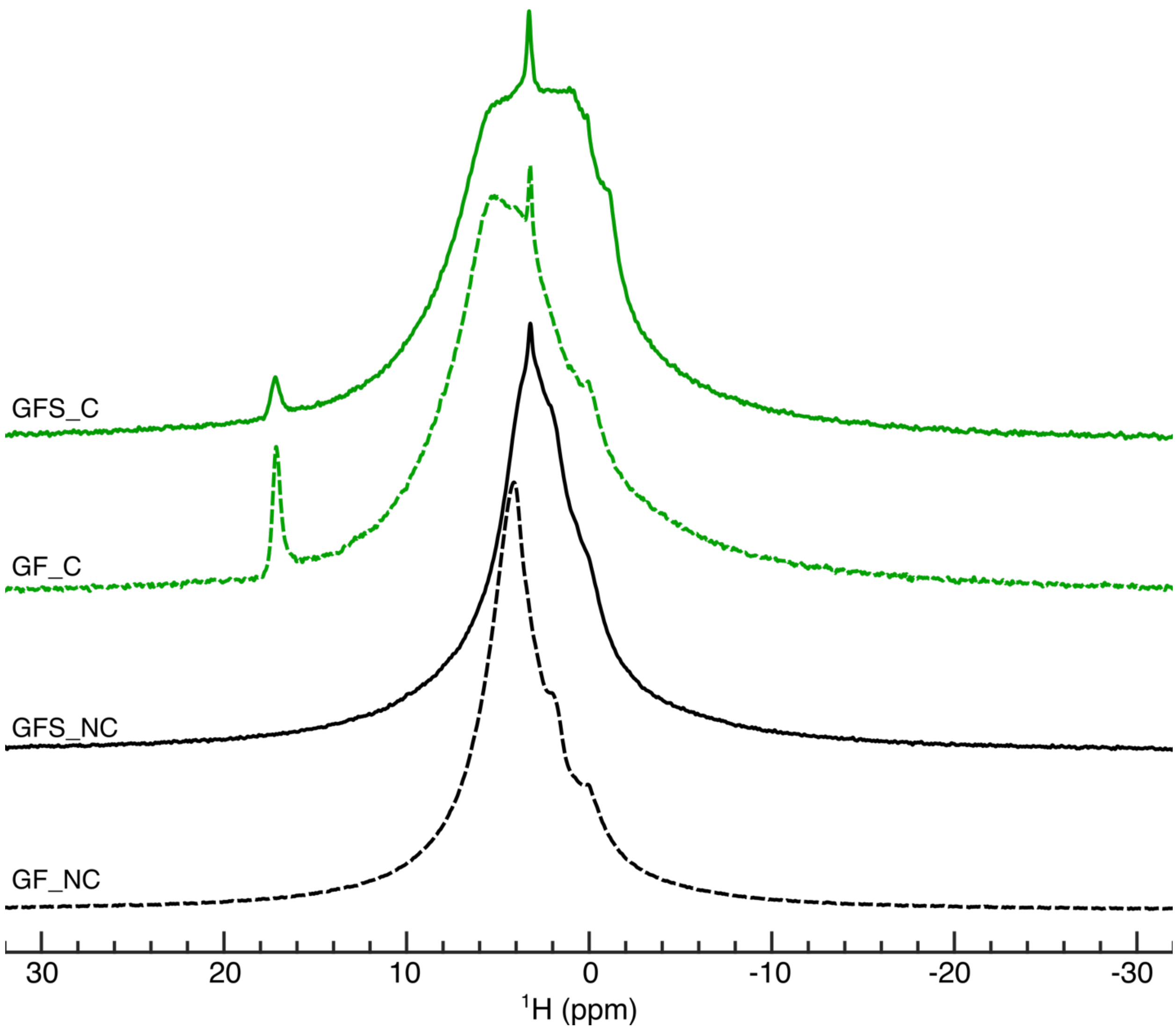

Fig. S6. ^{1}H MAS NMR spectrum at 9.4 T and 35 kHz MAS.
^{1}H MAS NMR spectra for the GF samples are shown in dashed lines and the GFS in solid lines. Black color represents the non-carbonated samples, whereas the spectra for the carbonated samples are shown in green.

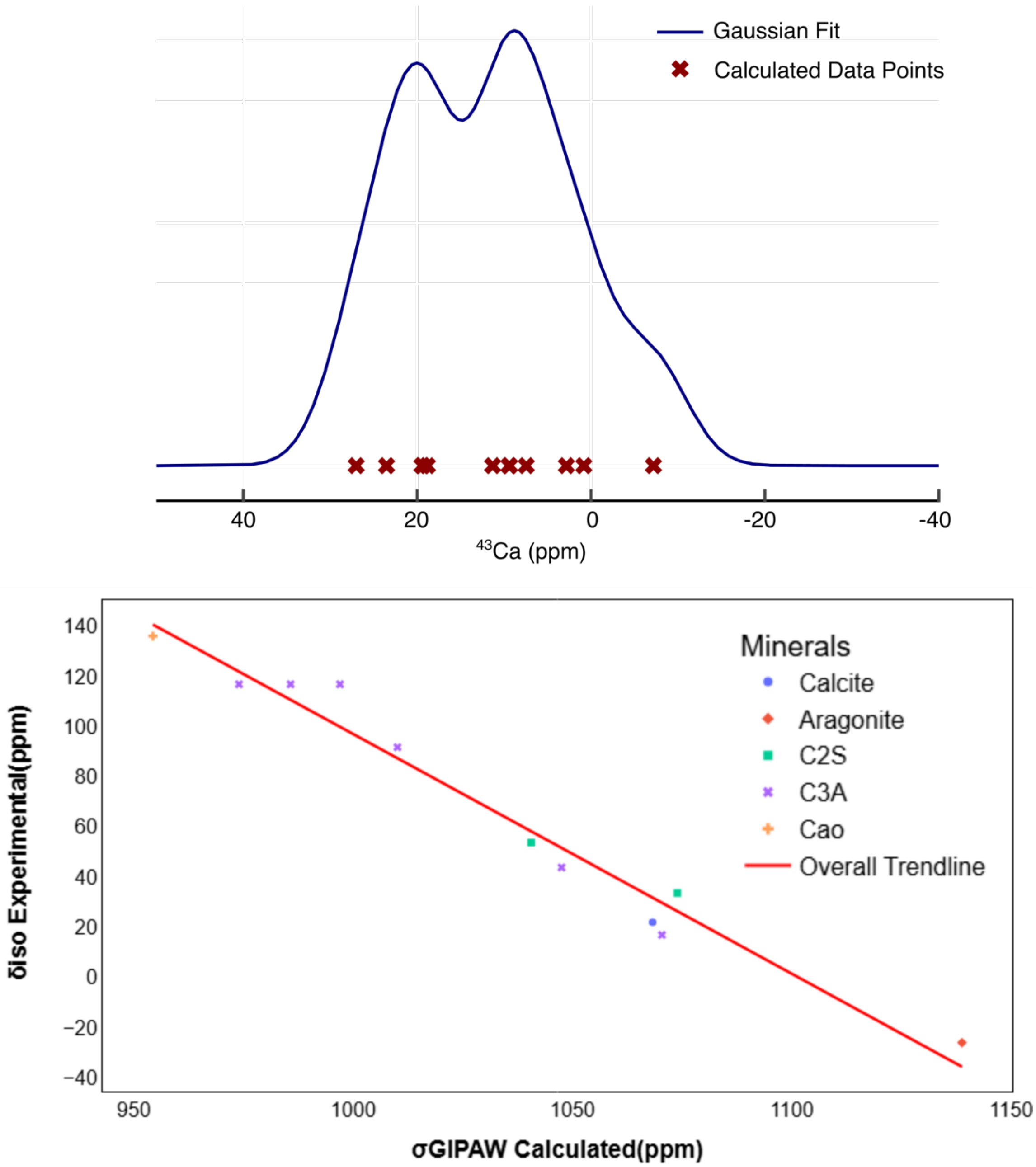

Fig. S7. Simulated ^{43}Ca chemical shifts for C-A-S-H (Ca/Si = 0.8)
^{43}Ca NMR chemical shift calculated for the C-A-S-H structures with Ca/Si = 0.8 and aluminum in all the three coordination as reported in Figure 4 in the manuscript.

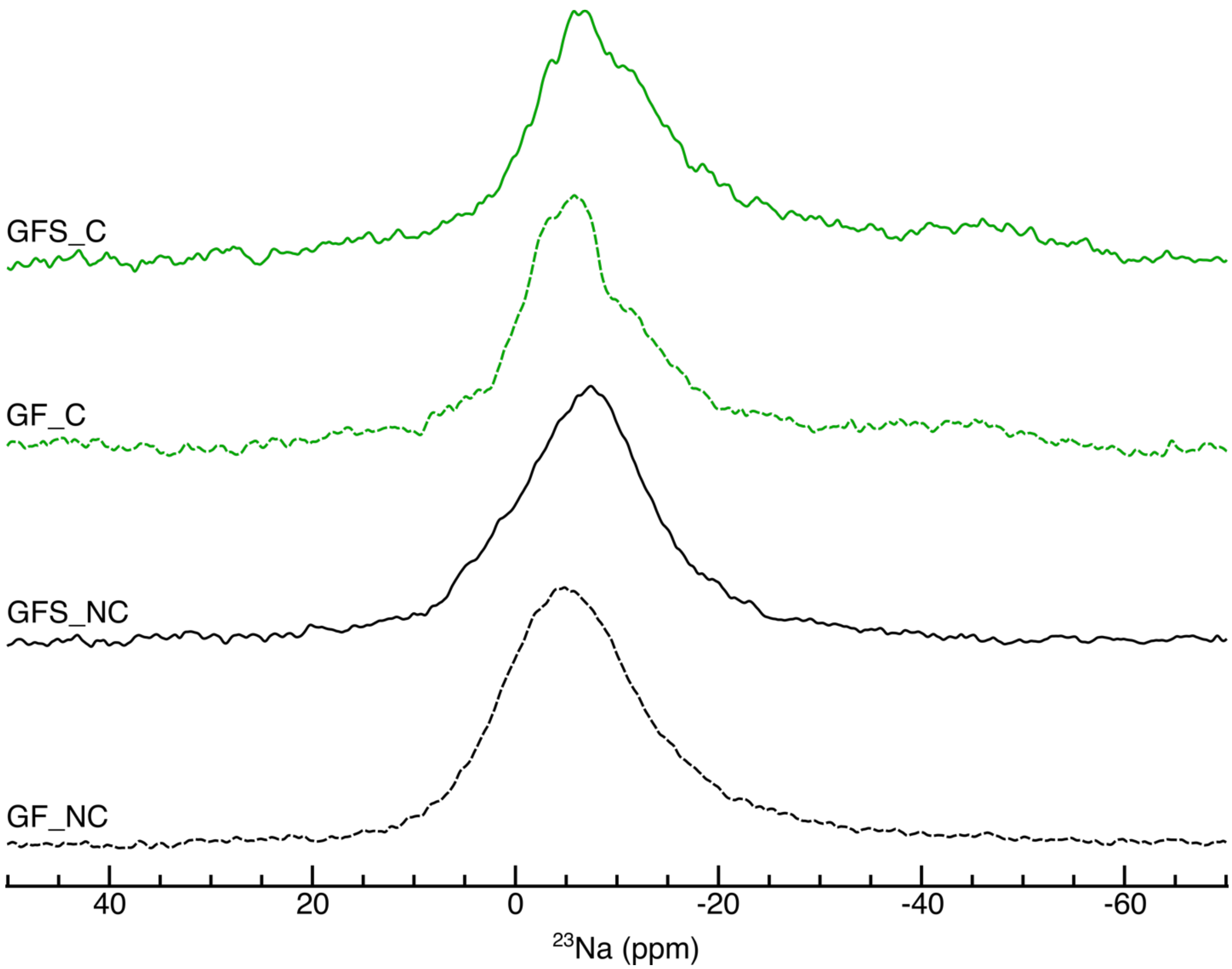

Fig. S8. ^{23}Na MAS NMR spectrum at 9.4 T and 30 kHz MAS.
^{23}Na MAS NMR spectra for the GF samples are shown in dashed lines and the GFS in solid lines. Black color represents the non-carbonated samples, whereas the spectra for the carbonated samples are shown in green.

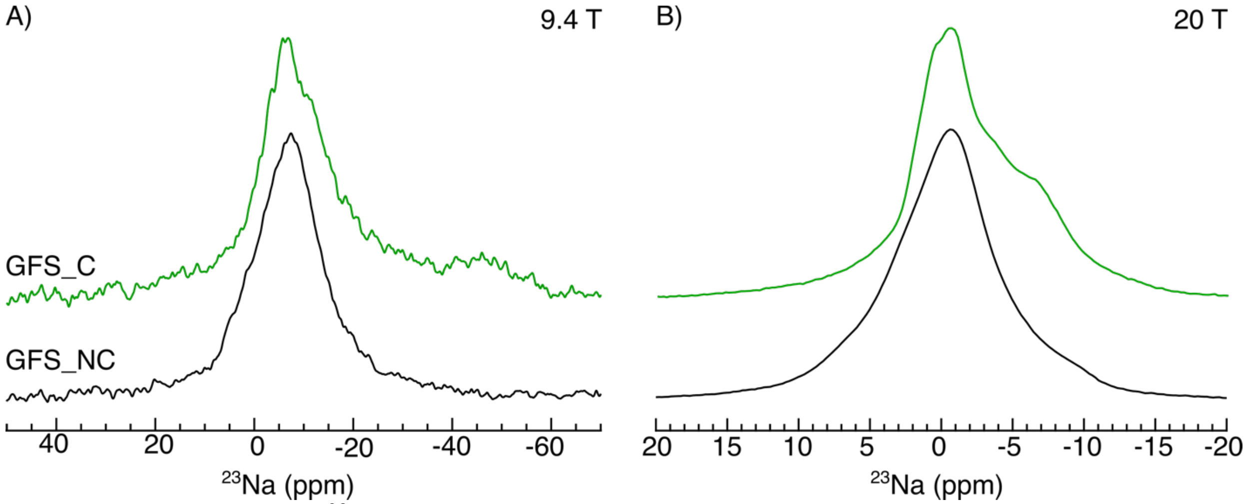

Fig. S9. Comparison of ^{23}Na MAS NMR spectra for GFS_NC and GFS_C.
The ^{23}Na spectra for GFS_NC (black) and GFS_C (green) samples recorded at (A) 9.4 T, 30 kHz MAS and (B) 20 T, 16 kHz MAS.

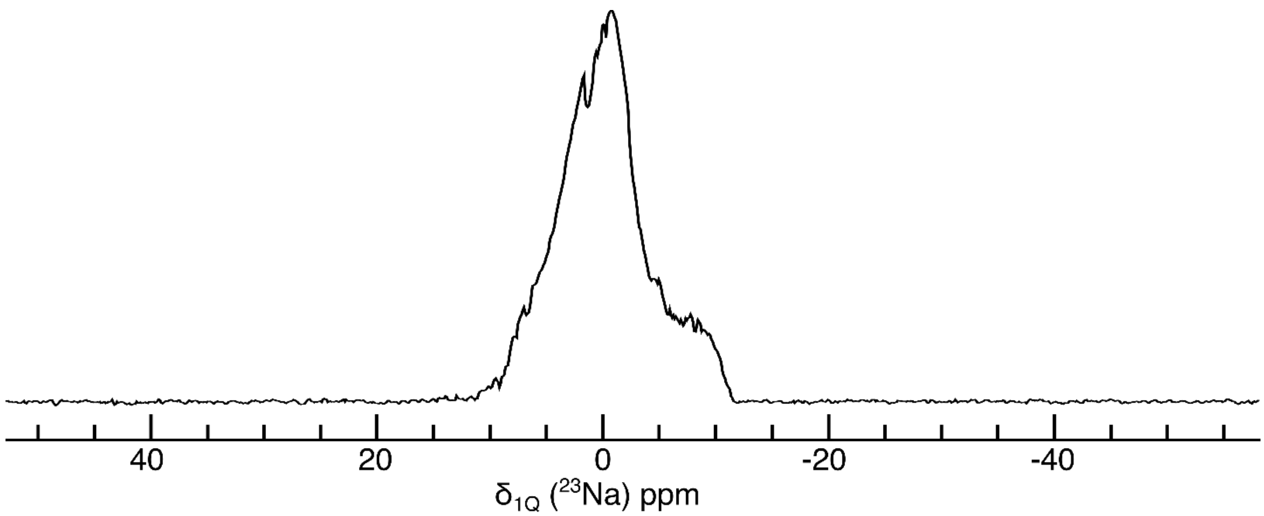

Fig. S10. 1D projection of ^{23}Na 3QMAS spectrum for GFS_NC. The sum projection is taken from 1Q dimension of the 23Na 3QMAS spectrum**.**

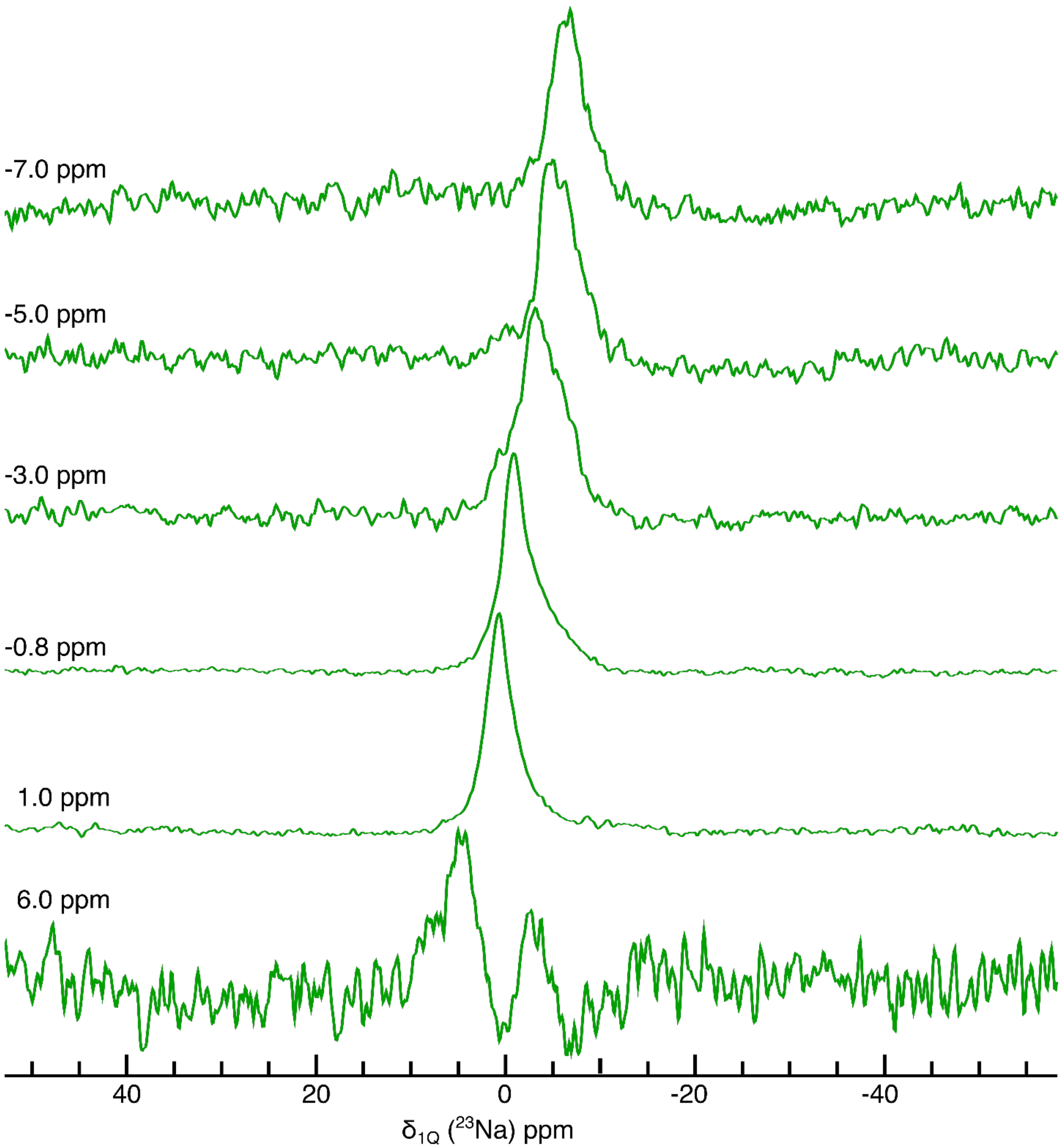

Fig. S11. Anisotropic slices from ^{23}Na 3QMAS spectrum for GFS_C. The slices were taken at different peak positions in the ^{23}Na 3QMAS spectrum.

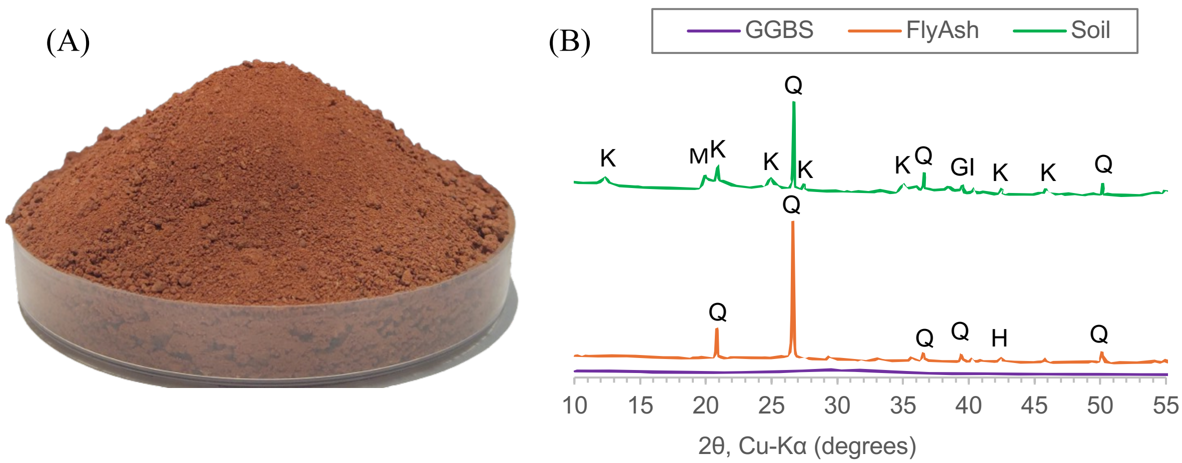

Fig. S12. XRD spectra for the soil

(A) laterite soil, (B) XRD of raw materials used in the experiments, K: Kaolinite, M: montmorillonite, GI: gibbsite, Q: Quartz , H: hematite.

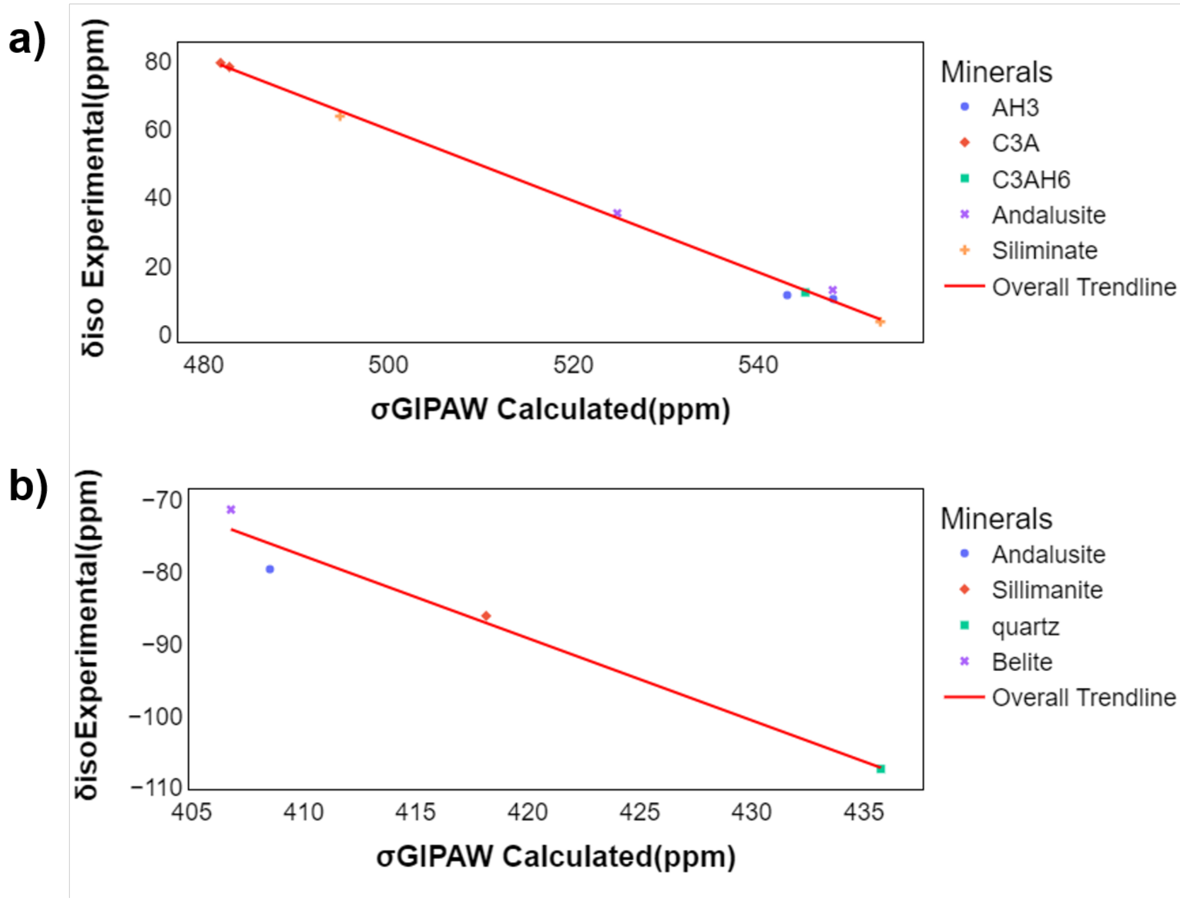

Fig. S13. Fitting for the ^{29}Si isotropic chemical shifts and shielding parameter.
Best fit to a line between the experimental isotropic chemical shifts and calculated isotropic shielding of (A) aluminate and (B) silicate minerals.

Table S1. Fit parameters of ^{27}Al MAS NMR spectra for GF_NC, GFS_NC, GF_C, and GFS_C

Site	Sample	δ_{iso} (ppm)			C_Q (kHz)			η_Q			LB (kHz)			Relative amount		
		I	II	III	I	II	III	I	II	III	I	II	III	I	II	III
Al(IV)	GF_NC	60	61	74	187	1481	160	0.253	0.119	0.17	0.4	1.3	0.8	0.23	0.75	0.02
	GFS_NC	57	60	62	80	108	1061	0.393	0.338	1.0	0.6	0.5	2.5	0.1	0.39	0.51
	GF_C	57	58	–	121	1578	–	0.032	0.051	–	1.4	3.8		0.28	0.72	–
	GFS_C	57	60	62	210	15	341	0.888	1.0	0.201	1.3	0.7	4.3	0.26	0.01	0.73
Al(VI)	GF_NC	9	10	11	233	1442	961	0.015	0.006	0.084	0.3	1.3	0.8	0.07	0.6	0.32
	GFS_NC	0	7	8	353	1844	1809	0.005	0.459	0.007	1.0	1.2	2.5	0.1	0.21	0.69
	GF_C	4	10	–	1169	1028	–	0.591	0.048	–	1.4	1.4		0.25	0.75	–
	GFS_C	0	1	11	3	113	238	0.975	0.89	0.439	1.4	2.5	1.8	0.17	0.24	0.59

Table S2. Calculated and calibrated values of ^{27}Al for different species of C-A-S-H.

Type of species	Calculated NMR (σ_{GIPAW}) value	Isotropic chemical shift (δ_{ref})
C-A-S-H Al(IV)	483.33	77.35
C-A-S-H Al(V)	527.29	31.45
C-A-S-H Al(VI)	552.02	5.12

Table S3. Calculated and calibrated values of ^{29}Si for different species of C-A-S-H.

Type of species	Calculated NMR (σ_{GIPAW}) value	Isotropic chemical shift (δ_{ref})
	409.82 (Q^2)	-77.53
	415.71	-84.27
C-A-S-H Al(IV)	416.15 (Q^2(1Al))	-84.78
	414.16	-82.62
	408.8 (Q^3(1Al))	-76.37
	414.46 (Q^2)	-82.84
	417.01	-85.76
C-A-S-H Al(V)	414.5 (Q^2(1Al))	-82.88
	413.76	-82.04
	426.10 (Q^3(1Al))	-96.16
	414.91 (Q^2)	-83.36
	417.20	-85.98
C-A-S-H Al(VI)	417.04 (Q^2(1Al))	-85.79
	414.74	-83.16
	411.65 (Q^3(1Al))	-79.63

Table S4. Fit parameters of ^{23}Na MAS NMR spectra for the GFS_NC and GFS_C sample.

Sample	δ_{iso} (ppm)	LB (kHz)	xG/(1-x)L	Relative Amount
GFS_NC	-8.0	1.2	0.3	0.06
	-4.0	1.3	0.7	0.11
	-0.2	1.2	0.7	0.53
	4.0	1.9	0.5	0.30
GFS_C	-7.0	1.1	0.0	0.23
	-5.0	0.5	0.0	0.02
	-3.0	0.8	0.0	0.18
	-0.8	0.5	0.8	0.12
	1.0	0.8	0.0	0.40
	6.0	1.5	0.0	0.05

Table S5. Significant bands in the FTIR spectra for GF and GFS sample

Wavenumber (cm^{-1})	Bands	Assignment
600-400	Si –O–X (X=Si/Al)	Bending vibrations[2,3]
620-500	Al–O	Stretching vibrations in Al(VI)[2]
870	C–O	Bending vibrations of O–C–O in CO_3^{2-}.[4]
970	Si–O	Stretching vibrations of Q^2 tetrahedra[4,5]
900- 700	Al–O	Stretching vibrations in Al(IV)[2]
1300-850	Si –O–X (X=Si/Al)	Asymmetric and symmetric stretching vibration in aluminosilicates[3,6]
1490-1410 1490 1430-1410	–C–O	Stretching vibration of CO_3^{2-} Vaterite Overlapping bands of vaterite and calcite[7]
1650	H–O–H	Bending vibrations[8]

Table S6. Oxide composition (%) of GGBS, FA, and clay and silt fraction of soil (<75 µm)

Raw materials	CaO	SiO_2	Al_2O_3	Fe_2O_3	MgO	SO_3	K_2O	TiO_2	Other elements
GGBS	38.6	34.8	16.6	0.4	5.4	1.6	0.5	0.8	< 1.4%
FA	3.2	60.6	25.4	5.2	0.9	-	1.4	1.4	< 0.8%
Clay and silt fraction of soil	0.4	53.1	33.9	9.4	-	-	1.3	1.2	< 0.5%

Table S7. Mix composition of alkali-activated binders; NC: non-carbonated, C: carbonated					
Mix composition	**GGBS (g)**	**FA (g)**	**Soil, <75 µm (g)**	**8M NaOH (g)**	**Curing condition**
GF	75	25	0	74	NC, C
GFS	75	25	26	74	NC, C

References

1. Gan, Z. Measuring multiple carbon–nitrogen distances in natural abundant solids using R-RESPDOR NMR. *Chem. Commun.* 4712–4714 (2006) doi:10.1039/b611447d.
2. Fernández-Carrasco, L., Torrens-Martín, D., Morales, L. M. & Martínez-Ramírez, S. Infrared Spectroscopy in the Analysis of Building and Construction Materials. in *Infrared Spectroscopy - Materials Science, Engineering and Technology* 369–382 (Intech, 2012). doi:10.5772/2055.
3. García Lodeiro, I., Macphee, D. E., Palomo, A. & Fernández-Jiménez, A. Effect of alkalis on fresh C–S–H gels. FTIR analysis. *Cem. Concr. Res.* **39**, 147–153 (2009).
4. García-Lodeiro, I., Fernández-Jiménez, A., Blanco, M. T. & Palomo, A. FTIR study of the sol-gel synthesis of cementitious gels: C-S-H and N-A-S-H. *J. Solgel Sci. Technol.* **45**, 63–72 (2008).
5. Ping, Y., Kirkpatrick, R. J., Brent, P., McMillan, P. F. & Cong, X. Structure of Calcium Silicate Hydrate (C-S-H): Near-, Mid-, and Far-Infrared Spectroscopy. *J. Am. Ceram. Soc.* **82**, 742–748 (1999).
6. Panias, D., Giannopoulou, I. P. & Perraki, T. Effect of synthesis parameters on the mechanical properties of fly ash-based geopolymers. *Colloids Surf. A* **301**, 246–254 (2007).
7. Li, N., Farzadnia, N. & Shi, C. Microstructural changes in alkali-activated slag mortars induced by accelerated carbonation. (2017) doi:10.1016/j.cemconres.2017.07.008.
8. Rovnaník, P. Effect of curing temperature on the development of hard structure of metakaolin-based geopolymer. *Constr. Build. Mater.* **24**, 1176–1183 (2010).